

Towards Adapting Deep Visuomotor Representations from Simulated to Real Environments

Eric Tzeng^{*1}, Coline Devin^{*1}, Judy Hoffman¹, Chelsea Finn¹, Xingchao Peng²,
Sergey Levine¹, Kate Saenko², Trevor Darrell¹

Abstract—We address the problem of adapting robotic perception from simulated to real-world environments. For many robotic control tasks, real training imagery is expensive to obtain, but a large number of synthetic images is easy to generate through simulation. We propose a method that adapts visual representations using a small number of paired synthetic and real views of the same scene. Our model generalizes prior approaches and combines a standard in-domain loss, a cross-domain adaptation loss, and a contrastive loss explicitly designed to align pairs of images in feature space. We presume a synthetic dataset comprised of views that are a superset of a small number of real views, where the alignment may be either explicit or latent. We evaluate our approach on a manipulation task and show that by exploiting the presence of synthetic-real image pairs, our model is able to compensate for domain shift more effectively than conventional initialization techniques. Our results serve as an initial step toward pretraining deep visuomotor policies entirely in simulation, significantly reducing physical demands when learning complex policies.

I. INTRODUCTION

Deep reinforcement learning methods have shown remarkable performance and generality on tasks ranging from simulated locomotion to playing Atari games [1], [2], [3]. Such models can be learned end-to-end, mapping observed pixels directly to actions. A key question has been whether such methods can be extended for use in the real world, where brute-force exploration of a policy parameter space with physical agents is infeasible.

Recent efforts have shown promising results on real-world manipulation through end-to-end learning using architectures designed to minimize network size, as well as sophisticated policy search methods to structure training [4], [5]. Such structured training can greatly reduce the number of physical trials. However, effective generalization to varied environments and objects is difficult with such limited datasets. Substantially longer interactions produce better generalization, but at a cost in time and effort that makes it impractical to learn large motion skill repertoires [6]. In this paper we propose a complementary paradigm, which has the potential to remove these restrictions by transferring learned visual representations from synthetic simulated environments to the real world.

In both vision and robotics, it has long been a desirable goal to use synthetic rendered images to train models that are effective in the real world. Classically, hand-engineered features were designed to be invariant to the domain shift

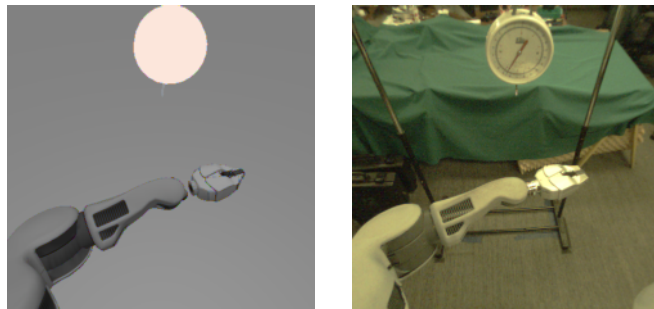


Fig. 1. A pair of corresponding synthetic (left) and real-world (right) images. Simply training a model on synthetic images and testing on real-world images yields poor performance due to differences in fidelity and inaccurate renderings. Despite these differences, by training on pairs like these, our method is able to learn from generated synthetic examples to perform robot manipulation in the real world. This enables learning of visuomotor policies without the need to collect large amounts of data for pre-training.

between synthetic and real worlds, e.g., efforts dating from the earliest model alignment methods in computer vision using edge detection-based representations [7]. It is especially notable that one of the earliest visuomotor neural network learning methods, ALVINN [8], exploited simulated training data of observed road shapes when training a multi-layer perceptron for an autonomous driving task. Many approaches to pose estimation in the recent decade were trained using rendered scenes from POSER and other human form rendering systems [9], [10], [11]; reliance on fixed feature representations limited their performance, however, and state-of-the-art pose estimation methods generally train exclusively on real imagery [12], [13].

Deep visual representations have been successfully trained from synthetic imagery [14], [15] and generally have a greater degree of domain invariance than conventional methods; nonetheless, as has been previously reported [16] and our experiments below confirm for visuomotor convolutional networks, even state of the art deep models are still typically suboptimal when trained on synthetic data and tested on real data.

Domain adaptation methods have been proposed in the literature to specifically optimize deep representations to be invariant to source-target domain bias in visual recognition tasks [17]. We propose a similar paradigm for training deep convolutional visuomotor models, including those that incorporate deep spatial feature points [4].

Existing deep domain adaptation methods have focused

^{*} Authors contributed equally.

¹ University of California, Berkeley

² University of Massachusetts Lowell

on the category-level domain invariance task, and employed optimization which generally reduced the discrepancy or confusion between domains; this is valuable, but misses a significant opportunity in the setting of synthetic to real image adaptation. It is often feasible to align a small number of real images to a simulated environment, which provides instance level training constraints for a deep domain adaptation architecture. While such constraints have been explored in earlier adaptation schemes (e.g. [18]), to our knowledge they have not been combined with contemporary deep discrepancy or deep confusion models. We propose a novel generalized framework, with losses for both pairwise and distribution alignment, and illustrate performance gains on robot-related pose estimation tasks. We also introduce a method for aligning real-world imagery with renderings produced by a simulator without relying on pose annotations, thereby alleviating the need for instrumented setups.

We report experiments with our framework on the pose pretraining stage of the visuomotor model of [4], using a real and simulated PR2, as shown in Figure 1. We also evaluate the learned representations by using them as input for training a visuomotor policy. Our results confirm (1) there is a significant domain shift between synthetic and real settings in visuomotor task learning, (2) that domain adaptation methods specialized to the deep spatial feature point architecture can learn to be relatively invariant to such shifts and improve performance, and (3) that inclusion of pairwise constraints provides a performance boost relative to previous deep domain adaptation approaches based solely on discrepancy minimization or domain confusion maximization. We show that, even in settings where pose annotations are unavailable for real-world imagery, annotations can be transferred from a synthetic dataset generated by a low-fidelity renderer. Finally, we demonstrate that the visual representations learned by our method successfully enable learning of control policies without the need for pose-annotated real imagery, and validate our method by training a visuomotor policy on the PR2 to perform a simple manipulation task. As increasingly sophisticated simulation environments become integrated into our system, we expect our model to support simulated training of nearly the entire deep visuomotor pipeline, significantly reducing physical demands when training complex new tasks.

II. RELATED WORK

Our method is related to past work in domain adaptation, Siamese networks and policy learning.

Domain adaptation. We cast the shift from synthetic to real images as a domain adaptation problem. Classical visual domain adaptation methods tackled the problem where a fixed representation extraction algorithm was used for both visual domains and adaptation took the form of learning a transformation between the two spaces [18], [19], [20] or regularizing the target domain model based on the source domain [21], [22]. Further models improved upon this by proposing adaptation which both transformed the representation spaces and regularized the target model using the

source [23], [24]. Since the resurgence in the popularity of convolutional networks for visual representation learning, adaptation approaches have been proposed to optimize the full target representation and model to better align with the source, for example by minimizing the maximum mean discrepancy [25], [26] or by minimizing the a-distance (specific form of discrepancy distance [27]) between the two distributions [28], [17].

Recently, a method has been proposed to use 3D object models to render synthetic training examples for training visual models with limited human annotations needed [29]. It was shown that there is a specific domain shift problem that arises when applying a synthetically trained visual model to the real world data. This paradigm of synthetic to real was further used to study deep representations and what they learn by [30].

Contrastive Loss for adaptation. It has been shown that a contrastive loss between the source and target points is an effective technique for transferring information. A contrastive metric learning loss was used for training a transformation from source to target domain for visual domain adaptation in [31] and [18]. In those methods the learned adaptation was a kernelized transformation over a fixed representation. Earlier work introduced Siamese networks [32], [33] for which a shared representation is directly optimized using the contrastive loss for signature and face verification and later for dimensionality reduction [34] and person hand and head pose alignment [11]. [11] further explored combining synthetic data along with real data to improve representation invariance and overall performance, however this method used the synthetic data to regularize the learning of the real model and found that performance suffered once the amount of simulated data overwhelmed the amount of real world data. In contrast, our approach uses synthetic data to learn a complete model and uses a very limited number of real examples for refining and adapting that model.

Visuomotor policy learning. The standard approach to processing visual input for robotic control is to use a discrete state estimation system to distill the visual signal into a low-dimensional state (e.g., the positions of objects in the world). This state is then used as a noisy input into the control policy [35]. Recently, there has been considerable interest in learning visuomotor policies directly from visual imagery using deep networks [36], [4], [37], [3]. This tight coupling between perception and control simplifies both the vision and control aspects of the problem, but suffers from the major limitation that each new task requires collection, annotation, and training on real world visual data in order to successfully learn a policy. To overcome this issue, we explore how simulated imagery can be adapted for robotic tasks in the real world. Directly applying models learned in simulation to the real world typically does not succeed [16], due to systematic discrepancies between real and simulated data. We demonstrate that our domain adaptation method can successfully perform state estimation for a real robotic task using minimal real world data, suggesting that adaption from simulation to the real world can be effective for robotic

learning.

III. GENERALIZED DOMAIN ALIGNMENT FOR VISUOMOTOR TRAINING

We propose a visuomotor representation that pretrains on easily available simulated image inputs and adapts to real image inputs using a few supervised examples. Our representation is a crucial step towards simulation training of policies that receive pixels and output control parameters.

We build upon the end-to-end architecture presented by Levine et al. (2015) for training deep visuomotor policies that can learn to accomplish tasks such as screwing a cap onto a bottle or placing a coat hanger on a rack. The method first pretrains a convolutional neural network on a pose estimation task, then finetunes this network with guided policy search to map from input image to action. Guided policy search is initialized with trajectories from a fully observed state (where the locations of both the manipulated and target object are known), but once learned, the policy only requires visual input at test time.

We propose that this entire network could be trained in simulation and transferred to the real world using our adaptive visual network. This would require simulating the robot and its dynamics, as well as approximate 3D models of the relevant objects. Training in simulation not only has the potential to significantly reduce training time, but also increase the variations seen during training. For example, although training a real PR2 with a thousand different objects would be infeasible to do by hand, we can programmatically generate thousands of different object models from CAD data and input them into the simulation. Since the rendering and dynamics are imperfect, we propose the use of domain adaptation to bridge the gap.

In this paper we focus on solving the first critical step of pretraining the deep spatial feature point architecture using synthetic examples and then transferring the representation for use with real imagery. Success at this task supports the feasibility of visual transfer from rendered robotic environments to the real world in realistic scenarios. We show that, using only 100 unannotated real images, we can leverage synthetic data to generate feature points good enough to train policies dependent on visual inputs.

A. Generalized domain alignment

Our method, generalized domain alignment (GDA), combines three core elements. The first is a standard pose estimation loss which ensures the network correctly performs the pose estimation task. The second is a domain confusion loss to align the synthetic and real domains in feature space. Finally, the third is a contrastive loss to align specific pairs in feature space. Together, these three losses ensure that we learn a representation that is conducive to the pose estimation task while remaining robust to the synthetic-real domain shift. Our model is novel in that it is the first deep adaptive model to explicitly exploit pairs of images to better mitigate domain shift and learn domain invariant representations.

Pose estimation loss. The first loss function our method employs is a standard Euclidean loss on pose predictions. Given input images x and ground truth poses ϕ , we look to learn a representation θ_{repr} and a pose regressor θ_ϕ that minimizes the following pose estimation loss:

$$\mathcal{L}_\phi(x, \phi; \theta_\phi, \theta_{\text{repr}}) = \frac{1}{2K} \sum_i \|\theta_\phi^T f(x^{(i)}; \theta_{\text{repr}}) - \phi^{(i)}\|_2^2. \quad (1)$$

Domain confusion loss. However, because images produced in simulation are generally of much lower fidelity than real-world images, we expect a pose estimator trained primarily on synthetic data to perform poorly when evaluated on real data. Thus, we would like to additionally ensure that the representation we learn, θ_{repr} , is resilient to the domain shift between synthetic and real images. To this end, we adopt the domain confusion loss introduced by [17]. This loss learns a domain classifier θ_D that attempts to correctly classify each image into the domain it originates from. It then attempts to learn a representation θ_{repr} such that the domain classifier cannot distinguish the two domains in feature space. This loss corresponds to the cross entropy loss between the predicted domain label of each image x and a uniform distribution over the D domains:

$$\begin{aligned} \mathcal{L}_{\text{conf}}(x_S, x_T, \theta_D; \theta_{\text{repr}}) = \\ - \sum_{x \in (x_S \cup x_T)} \sum_d \frac{1}{D} \log q_d(x, \theta_D, \theta_{\text{repr}}). \end{aligned} \quad (2)$$

Here, q corresponds to the domain classifier activations:

$$q(x, \theta_D; \theta_{\text{repr}}) = \text{softmax}(\theta_D^T f(x; \theta_{\text{repr}})) \quad (3)$$

Contrastive loss. Thus far we have modeled the synthetic-real shift as a standard visual domain adaptation problem, where the synthetic domain serves as our source, and the real-world domain serves as our target. However, unlike standard adaptation settings, the synthetic-real shift is unique in that it is possible to render a synthetic version of each real image. In doing so, we provide explicit examples of images that our representation should consider identical, thereby separating the irrelevant, domain-specific differences from the details relevant to performing pose estimation.

To incorporate these pairwise constraints between corresponding images, we employ a modified version of the contrastive loss function introduced by [34]. As typically formulated, this loss function seeks to draw paired images closer together in feature space while ensuring that unpaired images remain separated. However, our synthetic dataset often has many examples in similar poses to any particular real image, which means there are often many other valid synthetic-real pairs in the dataset that are not explicitly identified. The dissimilarity term in the contrastive loss function would force these unlabeled similar pairs to be dissimilar, thereby making the optimization poorly conditioned. Thus, we choose to omit this term in our optimization.

More formally, given a set P of pairs (i, j) such that $x_S^{(i)}$

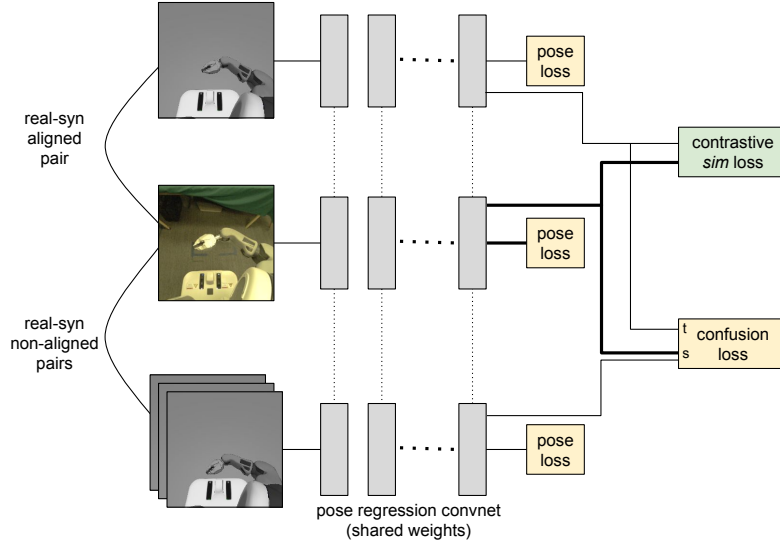


Fig. 2. Generalized domain alignment architecture.

and $x_T^{(j)}$ are paired, we write our contrastive loss as

$$\mathcal{L}_{\text{contrast}}(x_S, x_T, P, \theta_{\text{repr}}) = \sum_{(i,j) \in P} \left[\frac{1}{2} D(x_S^{(i)}, x_T^{(j)}; \theta_{\text{repr}})^2 \right] \quad (4)$$

where we define our distance function D as the Euclidean distance in the feature space corresponding to θ_{repr} :

$$D(x_S^{(i)}, x_T^{(j)}; \theta_{\text{repr}}) = \|f(x_S^{(i)}; \theta_{\text{repr}}) - f(x_T^{(j)}; \theta_{\text{repr}})\|_2. \quad (5)$$

Complete GDA objective. Our full model thus minimizes the joint loss function

$$\begin{aligned} \mathcal{L}(x_S, \phi_S, x_T, \phi_T, P, \theta_D; \theta_\phi, \theta_{\text{repr}}) = & \\ & \mathcal{L}_\phi(x_S, \phi_S; \theta_\phi, \theta_{\text{repr}}) + \mathcal{L}_\phi(x_T, \phi_T; \theta_\phi, \theta_{\text{repr}}) \\ & + \lambda \mathcal{L}_{\text{conf}}(x_S, x_T, \theta_D; \theta_{\text{repr}}) \\ & + \nu \mathcal{L}_{\text{contrast}}(x_S, x_T, P; \theta_{\text{repr}}) \end{aligned} \quad (6)$$

where the hyperparameters λ and ν trade off how strongly we enforce domain confusion and pairwise constraints.

We depict the architecture setup for a given sampled real image in Figure 2. For the target real image, we have access to an aligned synthetic image (*top image* Fig 2) as well as other synthetic images which are not necessarily aligned with the real image (non-aligned). The standard pose loss is applied to all images the network sees, regardless if they arise from synthetic or real processes. Each synthetic-real pair is input to the contrastive loss which seeks to make the points similar if they are aligned examples. Finally, all synthetic (source) examples as well as all real (target) examples are additionally optimized by the confusion loss, which seeks to make the representation agnostic to whether synthetic or real imagery was input to the network.

The combination of losses presented here is architecture-agnostic, thereby making our method applicable to many different pose estimation models. For this paper, we apply

our method to the deep spatial feature point network used by [4] to learn visuomotor policies for manipulation tasks.

Finally, we note that, while our discussion of our model here considers a pose estimation task, the combination of loss functions we present here is generic and can be applied to a variety of tasks including classification and detection, so long as paired source-target examples are present.

We implement our networks using the Caffe framework [38], and plan to release the code and datasets from our experiments upon acceptance of this paper.

B. Unsupervised pairing of synthetic and real imagery

Our method as presented thus far relies on the existence of pose annotations on the real-world imagery. However, in non-instrumented settings, it can often be impractical to collect the properly pose-annotated training data required to learn a visual representation for visuomotor policies. We therefore propose a method to mine weak pose annotations for our real-world imagery from our synthetic dataset. We learn a feature representation on the synthetic images and their pose annotations, then match real images to synthetic images via nearest-neighbor matching in this feature space. This enables us to obtain pose annotations for the real images by transferring them from the renderings produced by our simulator.

More precisely, we first train a network to perform pose estimation using only the pose annotations for the synthetic data. Once this synthetic-only pose network has been trained, we use it to extract the first convolutional response map for every image in our dataset, both real and synthetic. We perform max-pooling with a receptive field of 5, then compute a correlation score for each synthetic-real pair by taking the inner product of their pooled convolutional representations. Once these scores are computed, we simply pair each real image with the synthetic image with the highest correlation to it. This enables us to transfer pose

annotations between each pair of images, thereby annotating the real images.

We experiment with two methods of learning the initial alignment representation. The first simply trains the network to predict the pose of the synthetic renderings in our dataset. The second additionally utilizes the domain confusion loss [17] with the unlabeled real world data, ensuring that the representation produces similar features on both real and synthetic imagery. Regardless of the method used, because the network used to perform the alignment is trained to perform a pose estimation task, we expect that the resulting alignment will disregard irrelevant image features and focus primarily on the object whose pose we are trying to estimate.

C. Learning visuomotor control policies with adapted representation

Once we have assigned weak pose annotations to unlabeled real-world imagery as described in Section III-B, we can use the mined pairs to learn an invariant representation via GDA as described in Section III-A. This training process does not require any pose annotated real-world imagery and yields a visual representation that is robust to the synthetic-real domain shift and can effectively locate salient objects in a scene. We then use this learned representation to train a visuomotor control policy in the vein of previous work [5].

We use Guided Policy Search (GPS) with the adapted features to train a parametrized controller θ_{ctrl} . GPS turns reinforcement learning into a supervised learning problem by using time-varying linear controllers to collect (observation, control) data that is used to train a parametrized nonlinear controller. Since the system dynamics are unknown, we alternate between fitting linearized dynamics $p(x_{t+1}|x_t, u_t)$, collecting new trajectories $\{\tau\}$, and fitting the nonlinear controller to the (o, u) pairs in the trajectories.

Like in [5], we fit time-varying linear models to the robot joint states and use these to collect a dataset of feature points, feature point velocities, robot arm states, and joint efforts. The feature points are generated by the pose estimation network trained with GDA, and the optimization does not backpropagate through this network. As in [4], we used BADMM to jointly optimize the controllers and neural network with a penalty on the KL divergence between them. In Algorithm 1, u_t is the joint efforts at time t , x_t is the state of the robot and the position of the target, o_t is the state of the robot and the locations and velocities of the learned feature points $\theta_{\text{repr}}(\text{img})$, and θ_{ctrl} is the neural network trained to map from o to u . θ_{ctrl} is a 2-layer network with 40 hidden units per layer. Unlike in [5], we do not apply any filtering or smoothing to the feature points. The final result is a visuomotor control policy that is pretrained solely on unannotated real imagery and low-fidelity synthetic renderings. Examples of the training process and results are shown in a supplementary video¹.

Algorithm 1 GPS with adapted pose features

- 1: Train pose estimator θ_ϕ and θ_{repr} on labeled synth images
 - 2: Align unlabeled real and synth images as in Section III-B
 - 3: Retrain pose estimator with GDA
 - 4: Initialize trajectory distribution $p(u_t|x_t)$
 - 5: **for** iteration $k = 1$ to K **do**
 - 6: Run $p(u_t|x_t)$ to collect trajectory samples $\{\tau_i\}$
 - 7: Fit dynamics $p(x_{t+1}|x_t, u_t)$ to $\{\tau_i\}$ using linear regression with GMM prior.
 - 8: Fit $p(u|x)$ and θ_{ctrl} with an iteration of GPS
 - 9: **end for**
-

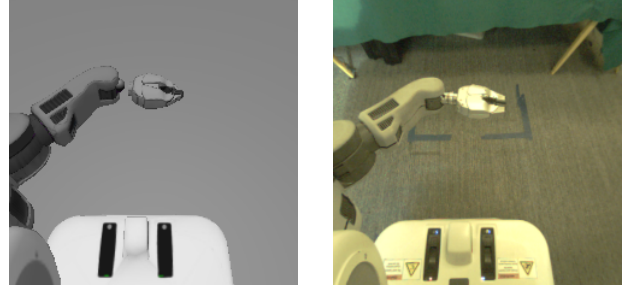


Fig. 3. A pair of corresponding synthetic (left) and real-world (right) images used for our pose estimation evaluation. The task is to predict the 3D pose of the PR2’s gripper.

IV. EVALUATION

We now empirically evaluate our method in a variety of experimental settings. We begin with an evaluation of GDA on a simple pose estimation task in Section IV-A. Next, we investigate the quality of synthetic-real pairings produced by our unsupervised alignment method in Section IV-B. Finally, we use the learned pairings to train a representation via GDA, then use this representation to train a full visuomotor control policy on a “hook loop” manipulation task in Section IV-C. These experiments demonstrate the effectiveness of incorporating synthetic imagery into the pretraining of visuomotor policies.

A. Robotic pose estimation

As a self-contained evaluation of our visual adaptation method, we first evaluate our method on a pose estimation task that is representative of the visual estimation required for robotic visuomotor control. We train a model to regress to the 3D location of three specific points on the robot gripper, thereby capturing its pose. We collected pose labeled images from the Gazebo simulator, where we can know the exact location of all objects. All positions are relative to the robot base, and all samples are rectified color images from the PR2’s right wide stereo camera. An example synthetic-real pair is shown in Figure 3.

For this task, we adopt the deep spatial feature point architecture introduced by [4]. Both the domain confusion loss ($\lambda = 0.1$) and contrastive loss ($\nu = 0.01$) are applied at the third convolutional layer, after the ReLU nonlinearity. As before, when both losses are employed simultaneously,

¹<https://youtu.be/wB26gyAAUoY>

Method	Average distance (cm)
Synthetic only	26.37
Real only	4.32
Synthetic and real	6.15
Domain confusion [17]	6.88
Contrastive loss	4.82
Generalized domain alignment	3.99
Oracle	0.94

TABLE I

EVALUATION RESULTS ON PR2 GRIPPER POSE ESTIMATION WHEN LIMITING OURSELVES TO ONLY 5 REAL EXAMPLES. ONCE AGAIN, EACH REAL EXAMPLE IS PAIRED WITH A CORRESPONDING SYNTHETIC IMAGE IN THE SAME POSE, AND AN ADDITIONAL 1000 UNPAIRED SYNTHETIC IMAGES ARE ALSO PROVIDED AS TRAINING DATA. THE MODEL IS TRAINED TO OUTPUT THREE 3D POINTS THAT DEFINE THE POSE OF THE GRIPPER, AND WE REPORT THE AVERAGE DISTANCE FROM THE GROUND TRUTH POINTS IN CENTIMETERS. WE FIND THAT, THROUGH COMBINING BOTH A DOMAIN CONFUSION LOSS AND A PAIR ALIGNMENT LOSS, WE ARE ABLE TO IMPROVE PERFORMANCE BY 10% (RELATIVE).

Setting	Synthetic only	Domain confusion [17]
Static camera	5.3 cm	5.3 cm
Head motion	13.1 cm	9.1 cm

TABLE II

AVERAGE ERROR FROM TRANSFERRING POSE ANNOTATIONS FROM SYNTHETIC TO REAL IMAGES USING OUR UNSUPERVISED ALIGNMENT METHOD OUTLINED IN SECTION III-B.

we further halve each of their weights. Results from this experimental setting are presented in Table I.

Once again, the results indicate that adaptation with paired examples yields improved performance. Interestingly, we find that despite how visually similar the synthetic and real images may appear, incorporating synthetic imagery during training is nontrivial. Simply combining synthetic and real imagery into one large training set negatively impacts performance, due to slight variations in appearance and viewpoint. We see that domain confusion alone does not help either, since domain confusion does not offer a way to learn the specific viewpoint variations between the real and synthetic domains. Nonetheless, by exploiting the presence of pairs, our method is able to account for these differences, performing better than all other baselines.

For additional experimental validation of our adaptation method, we refer the reader to our appendix, where we evaluate on a pose estimation task using both real-world PASCAL airplane instances and synthetic renderings of airplane CAD models.

B. Unsupervised synthetic-real alignment

To evaluate the effectiveness of our alignment method, we transfer pose annotations from paired synthetic images to their corresponding real images, then compute the error relative to the real-world ground truth pose annotations. In order to mimic a real control setting, we perform this experiment on the “hook loop” task introduced in [5], where

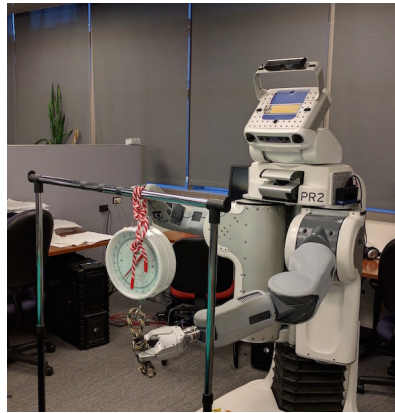


Fig. 4. In the “hook loop” task, the PR2 must position a loop of rope over the hook of a supermarket scale.

the robot is expected to place a loop of rope on a hook, as depicted in Figure 4. We generate low-fidelity renderings of the PR2 and a hook in 4000 different configurations and attempt to align these with 100 real-world images of the PR2 and a hook without pose annotations.

To learn the representation used for producing the alignment in this setting, we attempt to estimate the 3D pose of the target hook. We evaluate both the alignment produced using the simple synthetic-only model, as well as a model trained with an additional domain confusion loss. Table II shows the results of this experiment on two experimental settings: one with a fixed camera, and one in which the head of the robot (and the camera as well) moves around slightly. The relatively low error in the results indicates that the alignments are generally of high quality. Additionally, although we see no difference in the simple static camera setting, in the setting with head motion, we find that including the domain confusion loss decreases the error by over 30% relative, demonstrating the importance of adaptation techniques in this setting.

Visual inspection of the results also indicates that our method produces high-quality pairings. Figure 5 shows example results of our unsupervised alignment method in the static camera setting using the representation trained only on the synthetic data. The hooks in the synthetic renderings match quite closely with the hooks in the corresponding real images. We also find that, as expected, the position of the arm is largely ignored, and the alignment focuses primarily on the portion of the image that is relevant for the pose estimation task.

C. Visuomotor policies for the Hook Loop task

After determining the synthetic-real pairings using our method, we retrain the pose predictor on the combined data to learn the final feature points θ_{repr} . To evaluate these feature points, we set up the “hook loop” task from [5]. This task requires a PR2 to bring a loop of rope to the hook of a supermarket scale, as depicted in Figure 4. As the location of the scale is not instrumented, the robot must adjust its actions by visually perceiving the location of the hook/scale.

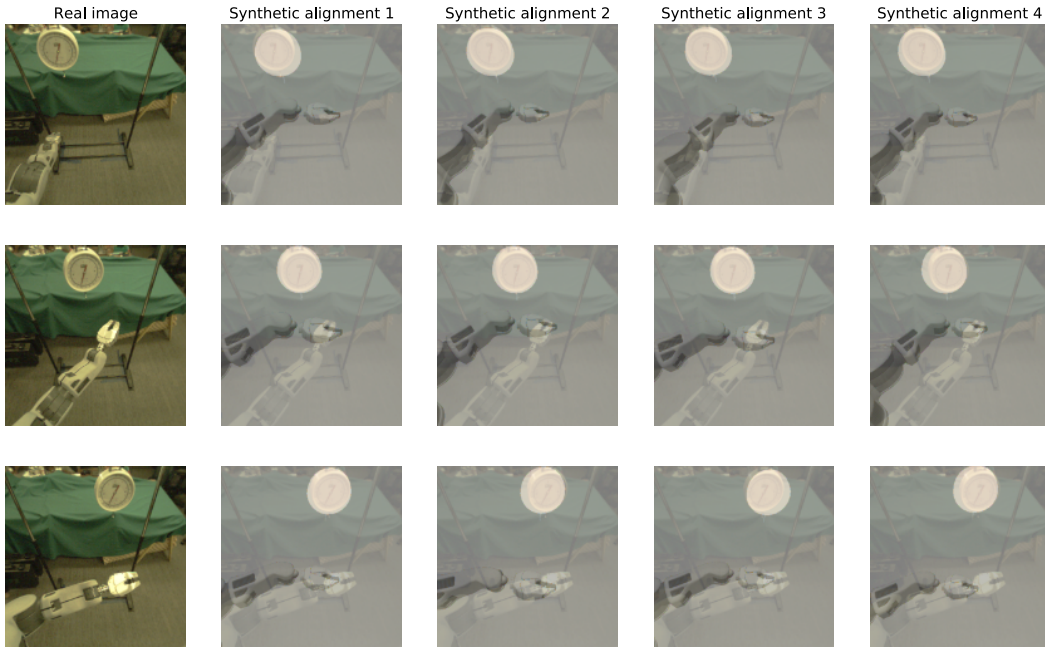


Fig. 5. Example alignments generated by our unsupervised synthetic-real alignment method in the static camera setting. The first column shows an example real image, and the next four columns show the top four corresponding images from our rendered dataset. We overlay a translucent version the real image on the synthetic images to better show the quality of our alignment. We find that, despite having no pose annotations on the real-world imagery, we are able to effectively find very close corresponding images from our synthetically-generated dataset. We also observe that our alignment explicitly disregards the pose of the robot arm, as it is irrelevant to the task, and focuses primarily on the location of the target hook.

We used four target hook positions along a bar to learn the linear dynamics and generate trajectories. Guided Policy Search was run for 12 iterations, where each iteration obtained 5 sample trajectories for each target hook position. The linear-quadratic controller was given only the arm joint state, while the neural network policy was given the arm joint state as well as the feature point (x, y) positions and velocities.

The performance of the final policy θ_{ctrl} was measured by running it 24 times: 3 times at each of 8 positions (including the target positions). Success was defined as the loop being on or touching the hook. As shown in Table III, the features learned with Generalized Domain Alignment allowed Guided Policy Search to learn a much more accurate policy.

We also trained an “Oracle” controller. The feature points used were from a pose estimation model trained directly on 500 real images with ground truth data, and GPS was run for 15 iterations instead of 12. This controller performed only marginally better than the one trained with adapted features on only 100 unlabeled real images.

Our last baseline was the Deep Spatial Autoencoder from [5]. When trained on only 100 real images, the policy learned from these features performed well with 70% accuracy. However, surprisingly, when trained on 500 images, the policy performed much more poorly, achieving a 40% success rate. We hypothesize this is due to the nature of the data. The hook is a prominent bright white circle, and so with few examples the model primarily focuses on reconstructing this circle. However, as we introduce more real imagery, the

Visual representation	Success rate
Synthetic only	37.5%
Autoencoder (100)	70.8%
Autoencoder (500)	41.7%
Generalized domain alignment	79.2%
Oracle	87.5%

TABLE III
PERCENT OF SUCCESSFUL ATTEMPTS AT PLACING A LOOP OF ROPE ON A HOOK AFTER TRAINING WITH 12 ITERATIONS OF GPS (SEE ALGORITHM 1).

autoencoder is forced to model the arm as well, which can take a much wider variety poses than the hook. Thus, with more data, the learned feature points are drawn away from the hook and onto the robot arm instead, thereby impairing performance on the manipulation task. If the target object in the task were a more subdued object, we expect that the autoencoder baseline would perform poorly even with only 100 examples. In contrast, because our method uses pose supervision, it focuses feature points on the object of interest, thereby disregarding task-irrelevant image features.

Because of the optimization that happens during Guided Policy Search, the performance of the final controller is dependent on the quality of the feature points that are passed in: if the feature points give θ_{ctrl} enough information about the position of the hook, then the controller will learn to use it. However, if the feature points are not consistent enough in where they activate (such as in the synthetic only case), the controller cannot learn a policy that takes the hook location into account. For example, when the controller failed a trial it



Fig. 6. An example synthetic rendering of an airplane (left) using the pose from an actual PASCAL airplane example (right).

put the loop at a possible hook position, but not at the current hook position. These results show that we can successfully learn visual features from synthetic data and a small number of unlabeled real images that are sufficient for control.

In contrast to our prior work, which required either ground truth pose labels for the real-world images [4] or fifty 100-frame videos for a total of 5000 images for unsupervised learning [5], our method only uses 100 unlabeled real-world images. Being able to use unlabeled images is important for for practical real-world robotic applications, where determining the ground truth pose of movable objects in the world with a high degree of precision typically requires specialized equipment such as motion capture.

V. CONCLUSION

In this paper, we present a novel model for domain adaptation that is able to exploit the presence paired source-target examples. Our model extends existing adaptation architectures by applying a well-established contrastive function in an adaptation setting for the first time. Because of its generality, our method is applicable to a wide variety of deep adaptation architectures and tasks. Through a pose estimation task, we experimentally validate the importance of using image pairs and show that they are integral to achieving strong adaptation performance. We also demonstrate the ability to adapt even in settings where pose annotations on real-world data is unavailable.

We address domain adaptation for visual inputs in the context of robotic state estimation. The tasks used in our robotic evaluation involve estimating information that is highly relevant for robotic control [39], as well as for pretraining visuomotor control policies [4]. While we show successful transfer of simulated data for learning real-world visual tasks, training full control policies entirely in simulation will also require tackling the question of physical adaptation, to account for the mismatch between simulated and real-world physics. Addressing this question in future work would pave the way for large-scale training of robotic control policies in simulation.

APPENDIX

To further demonstrate the applicability of our approach, we evaluate on a simple airplane azimuth estimation task. The PASCAL3D+ dataset [40] provides additional 3D annotations for 12 rigid categories in the PASCAL VOC 2012 dataset [41]. We focus on the first of these categories,

“aeroplane,” and consider the task of estimating the azimuth of airplanes relative to the camera viewpoint.

However, to simulate an adaptation setting, in which target data is limited, we train using only 17 real images and augment our training data with synthetic renderings of airplanes, similar to [30]. We use the pose annotations on these 17 training images to render 3D models in the same pose over simple sky backgrounds. An example of one of these pairs is provided in Figure 6. We additionally render 321 additional synthetic images using the poses from 321 real images, but do not include the corresponding real images themselves. The remaining 338 real images (which are not used to generate synthetic renderings) are used for evaluation.

As a simple experiment, we repurpose the standard architecture of [42], replacing the final 1000-way output with a simple 2-way output to regress to the sine and cosine of azimuth. We initialize our model using weights learned on the ImageNet dataset [43]. Both the domain confusion loss (weighted at $\lambda = 0.01$) and the contrastive loss (weighted at $\nu = 10^{-5}$), when in use, are applied to the 7th layer. When using both losses together, we further halve the weights applied to each, so that $\lambda = 0.005$ and $\nu = 5 \times 10^{-6}$.

We report the percentage of test examples localized within error thresholds of varying sizes in Table IV. The results indicate that incorporating explicit paired examples into the optimization leads to improved performance on this simple pose estimation task. We also find that, although the domain confusion loss and the contrastive loss perform similarly on their own, combining them provides a further performance increase, indicating that the two losses are complementary.

We can gain additional insight by examining performance is if we use all available real training data instead of limiting ourselves to only 17 examples, thereby eliminating the train-test domain shift. This serves as an upper bound, and would be achieved if our synthetic renders perfectly matched their corresponding real photographs. We refer to this baseline as the “Oracle” baseline. Table IV shows that adaptation with paired constraints is able to make up over 50% of the difference in performance over the simple non-adaptive baseline.

REFERENCES

- [1] V. Mnih, K. Kavukcuoglu, D. Silver, A. Graves, I. Antonoglou, D. Wierstra, and M. Riedmiller, “Playing Atari with deep reinforcement learning,” *NIPS ’13 Workshop on Deep Learning*, 2013.
- [2] J. Schulman, S. Levine, P. Moritz, M. Jordan, and P. Abbeel, “Trust region policy optimization,” in *International Conference on Machine Learning (ICML)*, 2015.
- [3] T. P. Lillicrap, J. J. Hunt, A. Pritzel, N. Heess, T. Erez, Y. Tassa, D. Silver, and D. Wierstra, “Continuous control with deep reinforcement learning,” *arXiv preprint arXiv:1509.02971*, 2015.
- [4] S. Levine, C. Finn, T. Darrell, and P. Abbeel, “End-to-end training of deep visuomotor policies,” *CoRR*, vol. abs/1504.00702, 2015.
- [5] C. Finn, X. Tan, Y. Duan, T. Darrell, S. Levine, and P. Abbeel, “Deep spatial autoencoders for visuomotor learning,” in *International Conference on Robotics and Automation (ICRA)*, 2016.
- [6] L. Pinto and A. Gupta, “Supersizing self-supervision: Learning to grasp from 50k tries and 700 robot hours,” *arXiv preprint arXiv:1509.06825*, 2015.

Method	Accuracy at θ				Average
	$\theta = \frac{\pi}{4}$	$\theta = \frac{\pi}{8}$	$\theta = \frac{\pi}{16}$	$\theta = \frac{\pi}{24}$	
Synthetic only	39.94%	22.19%	11.83%	7.69%	20.41%
Real only	44.08%	22.49%	11.83%	9.76%	22.04%
Synthetic and real	46.15%	25.15%	12.13%	9.17%	23.15%
Domain confusion [17]	48.22%	27.81%	16.27%	10.36%	25.67%
Contrastive loss	47.63%	28.40%	16.57%	10.65%	25.81%
Generalized domain alignment	48.82%	30.18%	18.93%	13.02%	27.73%
Oracle	56.21%	34.91%	18.05%	13.31%	30.62%

TABLE IV

EVALUATION RESULTS ON PASCAL AIRPLANE POSE ESTIMATION WHEN LIMITING OURSELVES TO ONLY 17 REAL EXAMPLES. EACH REAL EXAMPLE IS PAIRED WITH A CORRESPONDING SYNTHETIC IMAGE IN THE SAME POSE, AND AN ADDITIONAL 321 UNPAIRED SYNTHETIC IMAGES ARE ALSO PROVIDED AS TRAINING DATA. EACH COLUMN REPORTS THE PERCENTAGE OF EXAMPLES CORRECTLY ESTIMATED WITH ERROR LESS THAN SOME ANGLE THRESHOLD θ . WE SEE THAT THE METHODS THAT CAN MAKE USE OF PAIRED SYNTHETIC AND REAL IMAGES OUTPERFORM OTHER STANDARD ADAPTATION METHODS. WE ALSO SEE THAT PAIR-BASED ADAPTATION PERFORMANCE BEGINS TO APPROACH THE “ORACLE” RESULT TRAINED ON 338 REAL EXAMPLES.

- [7] R. Brooks, R. Greiner, and T. Binford, “The acronym model-based vision system,” in *International Joint Conference on Artificial Intelligence* 6, 1979, pp. 105–113.
- [8] D. Pomerleau, “ALVINN: an autonomous land vehicle in a neural network,” in *Advances in Neural Information Processing Systems (NIPS)*, 1989.
- [9] G. Shakhnarovich, P. Viola, and T. Darrell, “Fast pose estimation with parameter-sensitive hashing,” in *Computer Vision, 2003. Proceedings. Ninth IEEE International Conference on*. IEEE, 2003, pp. 750–757.
- [10] R. Urtasun and T. Darrell, “Sparse probabilistic regression for activity-independent human pose inference,” in *Computer Vision and Pattern Recognition, 2008. CVPR 2008. IEEE Conference on*, June 2008, pp. 1–8.
- [11] G. W. Taylor, R. Fergus, G. Williams, I. Spiro, and C. Bregler, “Pose-sensitive embedding by nonlinear nca regression,” in *Advances in Neural Information Processing Systems 23*, J. Lafferty, C. Williams, J. Shawe-Taylor, R. Zemel, and A. Culotta, Eds. Curran Associates, Inc., 2010, pp. 2280–2288.
- [12] A. Toshev and C. Szegedy, “DeepPose: Human pose estimation via deep neural networks,” *CoRR*, vol. abs/1312.4659, 2013.
- [13] J. J. Tompson, A. Jain, Y. Lecun, and C. Bregler, “Joint training of a convolutional network and a graphical model for human pose estimation,” in *Advances in Neural Information Processing Systems 27*, Z. Ghahramani, M. Welling, C. Cortes, N. Lawrence, and K. Weinberger, Eds. Curran Associates, Inc., 2014, pp. 1799–1807.
- [14] H. Su, C. R. Qi, Y. Li, and L. J. Guibas, “Render for cnn: Viewpoint estimation in images using cnns trained with rendered 3d model views,” in *The IEEE International Conference on Computer Vision (ICCV)*, December 2015.
- [15] X. Peng, B. Sun, K. Ali, and K. Saenko, “Learning deep object detectors from 3d models,” in *The IEEE International Conference on Computer Vision (ICCV)*, December 2015.
- [16] F. Zhang, J. Leitner, M. Milford, B. Upcroft, and P. Corke, “Towards Vision-Based Deep Reinforcement Learning for Robotic Motion Control,” *ArXiv e-prints*, Nov. 2015.
- [17] E. Tzeng, J. Hoffman, T. Darrell, and K. Saenko, “Simultaneous deep transfer across domains and tasks,” in *International Conference in Computer Vision (ICCV)*, 2015.
- [18] K. Saenko, B. Kulis, M. Fritz, and T. Darrell, “Adapting visual category models to new domains,” in *Proc. ECCV*, 2010.
- [19] R. Gopalan, R. Li, and R. Chellappa, “Domain adaptation for object recognition: An unsupervised approach,” in *Proc. ICCV*, 2011.
- [20] B. Gong, Y. Shi, F. Sha, and K. Grauman, “Geodesic flow kernel for unsupervised domain adaptation,” in *Proc. CVPR*, 2012.
- [21] J. Yang, R. Yan, and A. G. Hauptmann, “Cross-domain video concept detection using adaptive svms,” *ACM Multimedia*, 2007.
- [22] Y. Aytar and A. Zisserman, “Tabula rasa: Model transfer for object category detection,” in *IEEE International Conference on Computer Vision*, 2011.
- [23] L. Duan, D. Xu, and I. W. Tsang, “Learning with augmented features for heterogeneous domain adaptation,” in *Proc. ICML*, 2012.
- [24] J. Hoffman, E. Rodner, J. Donahue, K. Saenko, and T. Darrell, “Efficient learning of domain-invariant image representations,” in *International Conference on Learning Representations*, 2013.
- [25] E. Tzeng, J. Hoffman, N. Zhang, K. Saenko, and T. Darrell, “Deep domain confusion: Maximizing for domain invariance,” *CoRR*, vol. abs/1412.3474, 2014.
- [26] M. Long, Y. Cao, J. Wang, and M. I. Jordan, “Learning transferable features with deep adaptation networks,” in *International Conference in Machine Learning (ICML)*, 2015.
- [27] Y. Mansour, M. Mohri, and A. Rostamizadeh, “Domain adaptation: Learning bounds and algorithms,” in *COLT*, 2009.
- [28] Y. Ganin and V. Lempitsky, “Unsupervised domain adaptation by backpropagation,” in *International Conference in Machine Learning (ICML)*, 2015.
- [29] B. Sun and K. Saenko, “From virtual to reality: Fast adaptation of virtual object detectors to real domains,” in *British Machine Vision Conference (BMVC)*, 2014.
- [30] X. Peng, B. Sun, K. Ali, and K. Saenko, “Exploring invariances in deep convolutional neural networks using synthetic images,” *CoRR*, vol. abs/1412.7122, 2014. [Online]. Available: <http://arxiv.org/abs/1412.7122>
- [31] B. Kulis, K. Saenko, and T. Darrell, “What you saw is not what you get: Domain adaptation using asymmetric kernel transforms,” in *Proc. CVPR*, 2011.
- [32] J. Bromley, I. Guyon, Y. LeCun, E. Säckinger, and R. Shah, “Signature verification using a “siamese” time delay neural network,” in *Advances in Neural Information Processing Systems 6*, J. Cowan, G. Tesauro, and J. Alspector, Eds. Morgan-Kaufmann, 1994, pp. 737–744.
- [33] S. Chopra, R. Hadsell, and Y. LeCun, “Learning a similarity metric discriminatively, with application to face verification,” in *Computer Vision and Pattern Recognition, 2005. CVPR 2005. IEEE Computer Society Conference on*, vol. 1. IEEE, 2005, pp. 539–546.
- [34] R. Hadsell, S. Chopra, and Y. LeCun, “Dimensionality reduction by learning an invariant mapping,” in *Proc. Computer Vision and Pattern Recognition Conference (CVPR’06)*. IEEE Press, 2006.
- [35] P. Pastor, H. Hoffmann, T. Asfour, and S. Schaal, “Learning and generalization of motor skills by learning from demonstration,” in *International Conference on Robotics and Automation (ICRA)*, 2009.
- [36] M. Riedmiller, S. Lange, and A. Voigtlaender, “Autonomous reinforcement learning on raw visual input data in a real world application,” in *International Joint Conference on Neural Networks*, 2012.
- [37] M. Watter, J. Springenberg, J. Boedecker, and M. Riedmiller, “Embed to control: a locally linear latent dynamics model for control from raw images,” in *Advances in Neural Information Processing Systems (NIPS)*, 2015.
- [38] Y. Jia, E. Shelhamer, J. Donahue, S. Karayev, J. Long, R. Girshick, S. Guadarrama, and T. Darrell, “Caffe: Convolutional architecture for fast feature embedding,” *arXiv preprint arXiv:1408.5093*, 2014.
- [39] P. Pastor, M. Kalakrishnan, J. Binney, J. Kelly, L. Righetti, G. Sukhatme, and S. Schaal, “Learning task error models for manipula-

- tion,” in *IEEE International Conference on Robotics and Automation*, 2013.
- [40] Y. Xiang, R. Mottaghi, and S. Savarese, “Beyond pascal: A benchmark for 3d object detection in the wild,” in *IEEE Winter Conference on Applications of Computer Vision (WACV)*, 2014.
- [41] M. Everingham, L. Van Gool, C. K. I. Williams, J. Winn, and A. Zisserman, “The pascal visual object classes (voc) challenge,” *International Journal of Computer Vision*, vol. 88, no. 2, pp. 303–338, June 2010.
- [42] A. Krizhevsky, I. Sutskever, and G. E. Hinton, “ImageNet classification with deep convolutional neural networks,” in *Proc. NIPS*, 2012.
- [43] O. Russakovsky, J. Deng, H. Su, J. Krause, S. Satheesh, S. Ma, Z. Huang, A. Karpathy, A. Khosla, M. Bernstein, A. C. Berg, and L. Fei-Fei, “ImageNet Large Scale Visual Recognition Challenge,” *International Journal of Computer Vision (IJCV)*, vol. 115, no. 3, pp. 211–252, 2015.